agriculture

MDPI

Article

Artificial Neural Network-Based Seedling Phenotypic Information Acquisition of Plant Factory

Kaikang Chen [1,2], Bo Zhao [2], Liming Zhou [2] and Yongjun Zheng [1,*]

[1] Department of Electrical and Mechanical Engineering, College of Engineering, China Agricultural University, Beijing 100089, China; ckk@cau.edu.cn
[2] National Key Laboratory of Agricultural Equipment Technology, Chinese Academy of Agricultural Mechanization Sciences, Beijing 100083, China
* Correspondence: zyj@cau.edu.cn

Abstract: This work aims to construct an artificial neural network (ANN) ant colony algorithm (ACA)-based fine recognition system for plant factory seedling phenotypes. To address the problems of complexity and high delay of the plant recognition system in plant factories, first, multiple cameras at different positions are employed to collect images of seedlings and construct 3D images. Then, the mask region convolutional neural networks (MRCNN) algorithm is adopted to analyze plant phenotypes. Finally, the optimized ACA is employed to optimize the process timing in the plant factory, thereby constructing a plant factory seedling phenotype fine identification system via ANN combined with ACA. Moreover, the model performance is analyzed. The results show that plants have four stages of phenotypes, namely, the germination stage, seedling stage, rosette stage, and heading stage. The accuracy of the germination stage reaches 97.01%, and the required test time is 5.64 s. Additionally, the optimization accuracy of the process timing sequence of the proposed model algorithm is maintained at 90.26%, and the delay and energy consumption are stabilized at 20.17 ms and 17.71, respectively, when the data volume is 6000 Mb. However, the problem of image acquisition occlusion in the process of 3D image construction still needs further study. Therefore, the constructed ANN-ACA-based fine recognition system for plant seedling phenotypes can optimize the process timing in a more real-time and lower energy consumption way and provide a reference for the integrated progression of unmanned intelligent recognition systems and complete sets of equipment for plant plants in the later stage.

Keywords: artificial neural network; plant factory; plant phenotype; ant colony algorithm; MRCNN

Citation: Chen, K.; Zhao, B.; Zhou, L.; Zheng, Y. Artificial Neural Network-Based Seedling Phenotypic Information Acquisition of Plant Factory. *Agriculture* **2023**, *13*, 888. https://doi.org/10.3390/agriculture13040888

Academic Editor: Jaime Prohens

Received: 7 March 2023
Revised: 28 March 2023
Accepted: 12 April 2023
Published: 17 April 2023

1. Introduction

1.1. Background

The spread of COVID-19 has brought huge changes to people's lives. Among these changes, an increasing number of people are beginning to pay more attention to new models of vegetable production suitable for indoor cultivation. As a new type of planting method, plant factories can provide a stable supply of vegetables for urban residents. As an agricultural facility that artificially controls the cultivation environment, the plant factory planting mode can control various factors, such as indoor light, temperature, humidity, and carbon dioxide concentration, which has greatly alleviated the phenomenon of grain yield reduction caused by the reduction in urban arable land [1–3]. However, at present, plants in factories are still mainly cultivated by manual intervention, and there are problems such as many production links and complicated process equipment. Therefore, the intelligent improvement of plant factories has attracted the attention of many scholars.

As a highly technically integrated agricultural production system, plant factories are characterized by informatization, mechanization, and intelligence. Mechanization is the key to enhancing efficiency and reducing the cost of plant factories, but while the efficiency

of mechanization is improved, it causes inevitable physical damage to plants [4]. As one of the intelligent algorithms, the artificial neural network (ANN) can extract and analyze the characteristics of plant height, leaf area, biomass, color change, and physiological and biochemical indicators of crops by collecting plant images. In this way, the intelligent identification of plant phenotypes can be achieved in a timely, rapid, and nondestructive manner [5,6]. Ant colony algorithm (ACA) analyzes and decides the optimal timing of equipment linkage operations regarding the phenotypic characteristics of plants, thereby realizing the high-speed operation of plant factories [7–9].

1.2. Recent Related Work

In plant factories, analyzing plant phenotypes is an important way to determine plant growth conditions. However, using manual methods to analyze plant phenotypes is not only slow and error-prone but also labor-intensive. Therefore, many scholars use artificial intelligence algorithms to identify plant phenotypes and other growth characteristics. Jin et al. (2019) proposed a voxel-based CNN for corn stem and leaf classification and segmentation. The ability of this method to isolate the structural components of crop phenotypes utilizing deep learning was demonstrated [10]. Wu et al. (2019) used deep learning for fast, precise, and noninvasive measurements of optimal view planning pipelines. It was found that its flexibility and planning time was significantly better than stand-alone robots [11]. Nesteruk et al. (2021) proposed an image compression mechanism for data acquisition. The results showed that it had an obvious effect on the deviation of plant classification, disease identification, and phenology [12]. Yang et al. (2021) proposed a framework for intelligent detection and identification of plant stomata under feature weight transfer learning, and the results showed that this method was remarkably superior to existing methods [13]. Lv and Qiao (2020) constructed a deep belief network-based cognitive computing system model and applied it to the control of collaborative robots and related data testing. It was proven that the system was of high accuracy and security [14].

Through the research and analysis of the above scholars, it is found that most scholars apply artificial intelligence algorithms to extract relevant data features in plant phenotype analysis. However, under the background of plant factories, it is rare to analyze the phenotype of plant seedlings, and there are still many problems in plant factories, such as many production links and complicated process equipment. Therefore, artificial intelligence algorithms are introduced to acquire plant phenotypic information and optimize process timing, which is crucial to enhance the efficiency of plant factories.

1.3. Innovation and Organizational Structure

In summary, with plant factories being used today, the efficient cultivation of plants without damage is of great practical significance to the improvement of crop productivity. Therefore, in this work, aiming at the problems of many production links and miscellaneous process equipment in plant factories, multiple cameras at different locations are employed to collect seedling images and construct 3D images. Then, the MRCNN algorithm is innovatively introduced to analyze the plant phenotype, and the optimized ACA is adopted to optimize the process timing in plant factories so that a plant seedling phenotype fine management system based on ANN-ACA is established. Finally, its performance is demonstrated through experiments to provide a basis for the subsequent intelligent development of plant factories. The overall organizational structure of our work is as follows. Chapter 1 is the introduction, which describes the related development background of plant factories and related studies on plant phenotypes and proposes the innovation points and contributions of this work. In the second chapter, the methods are expounded. Multiple cameras at various locations are established to collect seedling images and design 3D images, and a fine management system of plant factory seedling phenotypes is established based on ANN-ACA. The third chapter is the results and discussion, where the experimental evaluation of the model performance is performed, and it is compared with different schemes for further discussion and analysis. The fourth chapter is the conclusion, which gives

a brief description of the research results, as well as the limitations of this research and future prospects.

2. Materials and Methodologies

2.1. Temporal Analysis of Spatial Structure and Process Management in Plant Factories

The plant factory is composed of different functional rooms, such as a cultivation workshop, nursery room, harvesting and storage room, machinery room (nutrient solution pipe, carbon dioxide cylinder, control equipment, etc.), and management room (Figure 1). From the analysis of the system structure, the plant factory is based on the peripheral structure and various functional units. The all-weather operation and intelligent management of the plant factory are ensured through the construction of subsystems such as the nutrient solution circulation and control system, multilayer 3D hydroponic cultivation system, air conditioning, and purification system, carbon dioxide gas fertilizer release system, artificial light source system, and computer automatic control system [15–18].

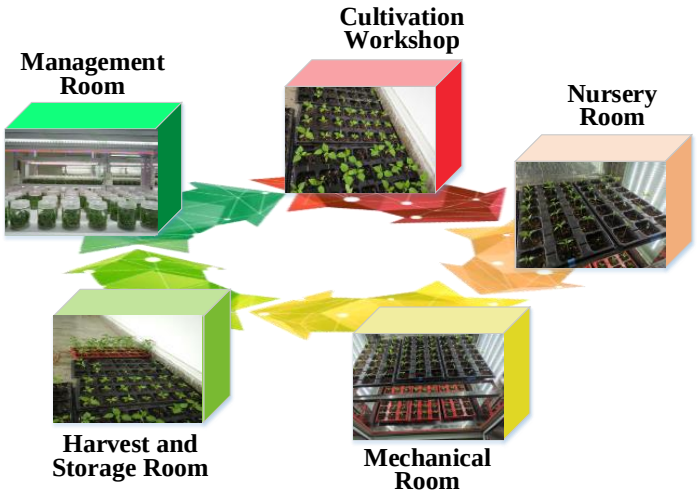

Figure 1. Spatial structure of the plant factory.

However, there are often problems of redundant production links and complicated process equipment in the practical adoption of plant factory models. Therefore, the key links and production factors of plant production in the plant factory are analyzed, and the phenotypic information of seedlings and the optimal timing rules of multi-equipment linkage operations in the factory environment are explored to realize the automatic production process and equipment linkage integrated control identification system, such as sowing, seedling raising, transplanting, harvesting, cleaning, packing, transporting, and stacking. It aims to provide a demonstration role for the development of the integration of intelligent identification systems and complete sets of equipment in unmanned plant factories.

2.2. ANN-Based Phenotype Analysis of Plant Seedlings

To accurately analyze the plant seedling phenotype of the plant factory, the ANN algorithm is employed. An extended form algorithm under Faster R-CNN, namely, the MRCNN algorithm, is selected. The algorithm can solve the orientation problem of the target image with semantic segmentation methods [19,20]. The MRCNN frame structure is shown in Figure 2.

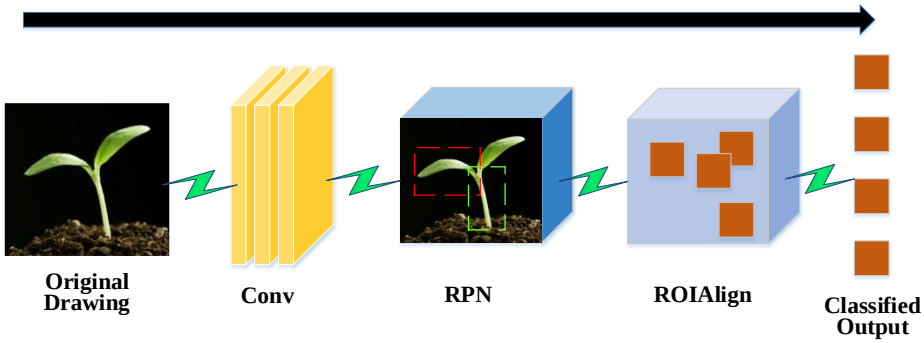

Figure 2. Frame structure diagram of MRCNN algorithm adopted to feature extraction of seedling images.

In Figure 2, the Faster R-CNN-based MRCNN algorithm is further integrated with the region proposal network (RPN) so that it can be well applied in complex life scenarios such as seedling phenotype recognition. ROIAlign determines the feature value of each point in the region of interest of the original image through bilinear interpolation and then performs pooling and other operations to improve the accuracy, providing a new solution to the misalignment alignment problem caused by pooling direct sampling [21]. In this algorithm, the backpropagation calculation is expressed as follows.

$$\frac{\partial L}{\partial x_i} = \sum_r \sum_j [d(i, i(r,j)) < 1](1 - \Delta h)(1 - \Delta w)\frac{\partial L}{\partial y_{rj}} \tag{1}$$

In Equation (1), y_{rj} refers to the j-th coordinate point of the r-th region after pooling, $i(r,j)$ refers to the original image point coordinates corresponding to point y_{rj}, and Δh and Δw refer to the gradients of the horizontal and vertical coordinates, respectively. Each grid can be defined as a *bin*, and the size of each *bin* is expressed as $\frac{w}{k} \times \frac{h}{k}$. The scoring equation for judging that the feature information on the (i,j)-th *bin* belongs to different categories is shown in Equation (2).

$$r_c(i,j|\Theta) = \sum_{(x,j)\in bin(i,j)} z_{i,j,c}(x + x_0, y + y_0|\Theta)/n \tag{2}$$

In Equation (2), $z_{i,j,c}$ refers to $k^2(c+1)$ outputs of a score map, the coordinates of the upper left corner of original region of interest are represented by (x_0, y_0), n is the pixel numbers in the *bin*, and Θ is the network parameters. Then, Equation (3) is obtained for each region of interest (ROI).

$$r(\Theta) = \sum_{i,j} r_c(i,j|\Theta) \tag{3}$$

Average score $r(\Theta)$ votes for each ROI. The MRCNN algorithm replaces the traditional SoftMax classifier with a sigmoid classifier, and the corresponding calculation equation is shown in Equation (4).

$$S(\Theta) = \frac{1}{1 + e^{-r_c(\Theta)}} \tag{4}$$

The expression of the loss function L is Equation (5).

$$L = L_{cls} + L_{box} + L_{mask} \tag{5}$$

In Equation (5), L_{cls} refers to the loss function in logarithmic form, and the classification corresponds to two categories: target and background. L_{box} refers to the loss function of the bounding box in the original image, and L_{mask} is the mean binary cross-entropy loss function, whose corresponding calculation equation is as follows.

$$L_{mask} = S(\Theta) = \frac{1}{1 + e^{-r_c(\Theta)}} \tag{6}$$

Therefore, according to Equation (6), the L_{mask} in the ROI of the $i(1 \leq i \leq c)$-th category is only related to the i-th L_{mask}, and the competition between different categories can be effectively avoided by corresponding to a mask for each class, thus improving the phenotype segmentation of seedlings. The loss principle of the multitask loss function is shown in Figure 3.

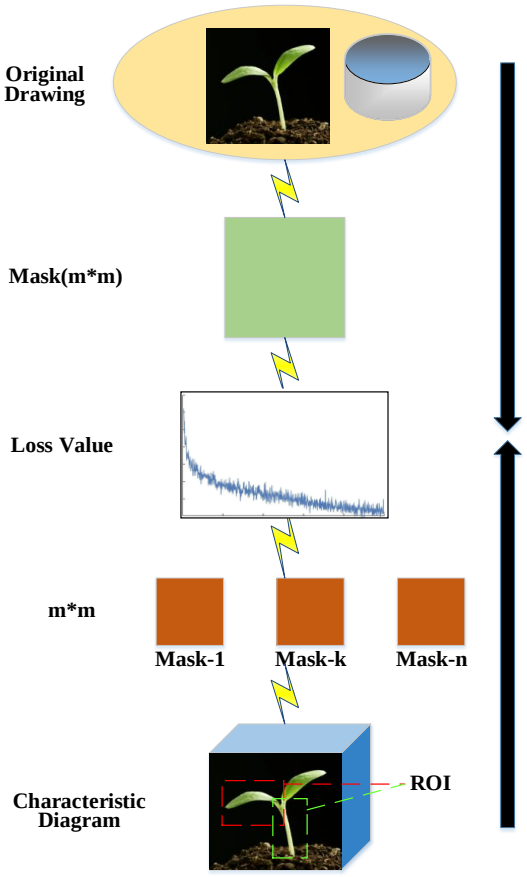

Figure 3. Schematic diagram of the multitask loss function in MRCNN.

From Figure 3, the mask feature predicted to be classified as k is obtained first regarding the original image, and then the mask area surrounded by the bounding box in the original image is mapped to the mask area feature of $m \times m$ size. Finally, the average binary cross-loss entropy of the $m \times m$ region is calculated and obtained.

In the seedling phenotype analysis, the center of the sponge conveyor belt in the phenotype acquisition area is set as the coordinate origin to further obtain more abundant and accurate information (Figure 4). The images of the seedlings are collected by using eight cameras (acA1300-30 gm, Basler, Arensburg, Germany) at different positions, and then the growth maps of the seedlings in different directions are plotted.

The key to the acquisition of seedling images is detecting different orientations of the seedlings, which currently mainly includes monocular and binocular vision detection algorithms [22,23]. The former represents the acquisition of seedling growth images by a camera. If point C is the camera, point P is the seedling in space, and the imaging point of the seedling in space is point $P'(u,v)$, then the angle between the projection of the camera's vertical perspective on the ground and the x- and y-axes of the horizontal ground is α, β. The mapping between the camera's horizontal perspective on the ground and the Y-axis of the ground plane is θ. Finally, Equations (7)–(9) are used to obtain α, β and θ, respectively.

$$\alpha = \arctan^{-1}\left(\frac{d}{y_b}\right) \tag{7}$$

$$\beta = \arctan^{-1}\left(\frac{d}{y_1 + y_b}\right) \tag{8}$$

$$\theta = \arctan^{-1}\left(\frac{x_1}{y_1 + y_b}\right) \tag{9}$$

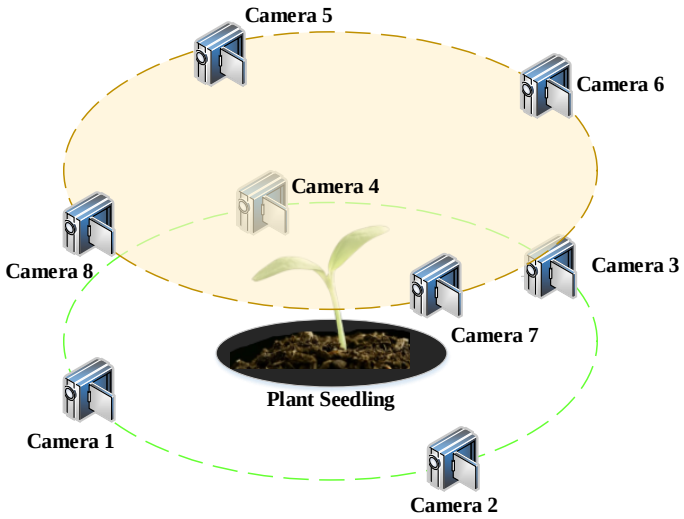

Figure 4. Camera placement diagram for image acquisition from different orientations of seedlings.

In the above equations, the distance from the camera to the ground is d, the shortest distance mapped to the ground from the vertical angle is y_b, and the longest distance is $y_1 + y_b$. Values of $d, y_1 + y_b, x_1$ are collected by measuring tools. S_x and S_y refer to the number of rows and columns of the images taken, respectively. The images taken are grayscale images of seedlings at different stages with a resolution of 1280 × 900 pixels. Where taking xoy as the coordinate system, y is the vertical distance between the seedling and the camera, x is the horizontal distance between the seedling and the camera, and L represents the actual distance between the seedling and the camera.

$$y = h \tan\left((90 - \alpha) + \left(1 + \frac{v}{S_y}\right) \times (\alpha - \beta)\right) \tag{10}$$

$$x = y \tan\left(\left(1 - \frac{v}{S_x}\right) \times \theta\right) \tag{11}$$

$$L = \sqrt{x^2 + y^2} \tag{12}$$

In binocular vision detection, the 3D coordinates of point $P(x_c, y_c, z_c)$ are shown in Equation (13):

$$\begin{cases} x_c = f\frac{BX_{left}}{Disprarity} \\ y_c = f\frac{BY}{Disprarity} \\ z_c = \frac{BY}{Disprarity} \end{cases} \tag{13}$$

Through monocular and binocular parallax analysis, it is revealed that the obtained images and seedling information have difficulty meeting the requirements of high real-time seedling growth. Therefore, for the acquisition of seedling phenotype images, an integral projection and region growing algorithm [24] fit for image position detection is adopted to detect the position of seedling in the first frame image. Machine learning algorithm is used for detection and analysis in real time to obtain accurate seedling phenotype information more efficiently.

In the integral projection coarse localization algorithm, $I(x, y)$ represents the pixel gray value of seedling image at point (x, y). The vertical and horizontal integral projection function $V(x)$ and $L(y)$ are used for calculation, as shown in Equations (14) and (15):

$$V(x) = \sum_{y=1}^{H} f(x, y), y = 1, 2, \cdots, H \tag{14}$$

$$L(y) = \sum_{y=1}^{W} f(x, y), x = 1, 2, \cdots, W \tag{15}$$

The horizontal and vertical integral projections are performed on these plant seedling images, and the midpoint of the obtained plant's coarse positioning position is set as seed point. Accurate seedling images are harvested by finely positioning seedlings using the region growing method. Eight cameras are used to obtain grayscale images of seedlings at different stages with a resolution of 1280 × 900 pixels. Background light is used to separate the seedling outlines from the background, and the seedling outlines generated from different cameras are merged. The resulting voxel spatial resolution is 0.25 mm/voxel, and the size is 240 × 240 × 300 voxels (*X*, *Y*, *Z*), corresponding to the actual 3D space of 60 × 60 × 76 mm. The 3D reconstruction speed is 20–60 ms per plant (i7-3.2 GHz processor is used); that is, the 3D point cloud model of approximately 10,000 seedlings is reconstructed every hour. In the acquisition of seedling images at different stages, it is agreed that the light condition is good, the temperature is kept between 18 and 22 degrees Celsius, and the relative humidity is kept between 40% and 70%, so that the effects of light and other environmental factors are ignored in the images of seedlings at different stages. The algorithm for obtaining 3D information of plant seedlings using multiple cameras with different orientations is shown in Algorithm 1.

Algorithm 1. Algorithm flow of 3D information acquisition of plant seedlings.

Start
Input: plant seedlings, 8 cameras in different directions
Output: 3D data information of plant seedlings
Rough location of seedlings by integral projection
Fine location of seedlings by regional growth method
Collecting plant seedling image $I_k, k \in \{1, 2, \cdots, 8\}$
For Image of each plant seedling I_k
$B_k \leftarrow$ foreground background segmentation (I_k)
for each voxel v of 3D space V
$V(v) \leftarrow 1$
End for
End for
For each voxel v of 3D space V
For each camera k
$i \leftarrow$ obtain the corresponding pixel (v, P_k)
If $B_k(i) =$ background
$V(v) \leftarrow 0$
Break
End if
End for
End for
End

After the 3D data information of the plant is harvested through the above algorithm flow, the shape of the stem and leaf of the plant seedling, petioles, and other small structural information can be visualized clearly (Figure 5). Thus, accurate plant seedling phenotype information can be obtained.

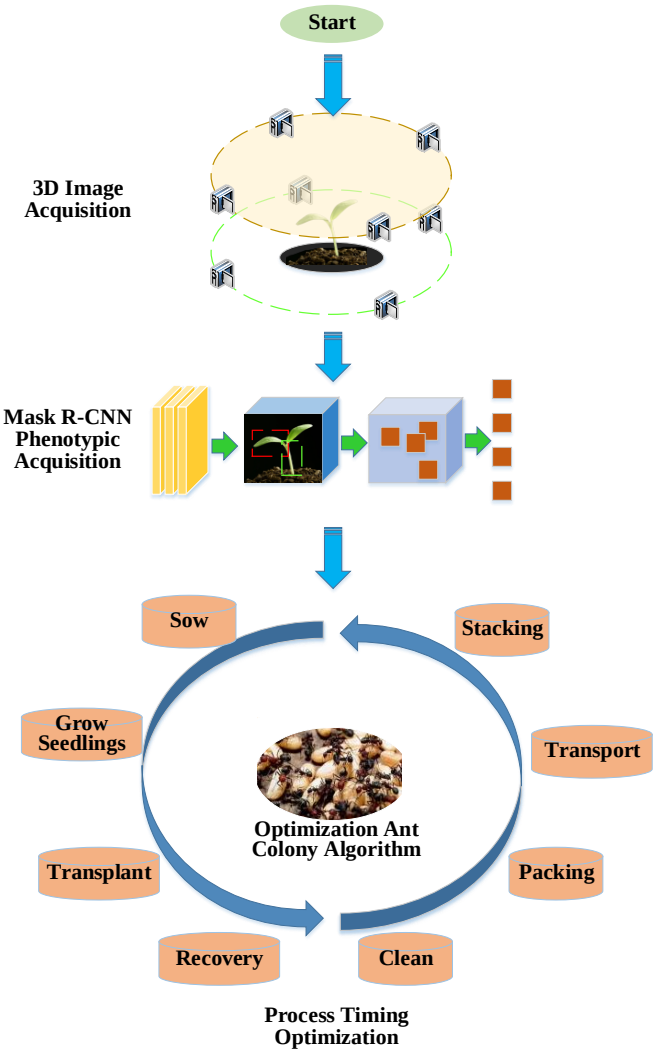

Figure 5. A framework for the fine identification system of plant seedling phenotype under ANN and ACA.

2.3. Optimization System Analysis of Plant Factory Seedling Phenotype Fine Management via Optimized ACA

After the identification of seedling phenotypes in plant factories, it is also critical to carefully manage plant growth according to the obtained phenotypic information. Therefore, the production operation control identification system in the plant factory is equipped and optimized to develop the "environment-quality-yield" intelligent and fine identification system. Figure 5 shows the framework of the ANN-ACA-based plant factory seedling phenotype fine identification system.

In Figure 5, first, the center of the sponge conveyor belt in the phenotype acquisition area is set as the coordinate origin, eight cameras at different positions are employed to collect the images of the seedlings, and a 3D image of the plant seedlings is constructed. Second, MRCNN is used to extract features in 3D images of seedlings. Among them, the mask R-CNN algorithm can complete the task of instance segmentation. Based on the input plant seedling image, it can provide the boundary box of each instance and segment the instance within the box to generate the instance mask to understand the plant seedling phenotype. Finally, the optimized ACA is used to optimize and solve the optimal timing of equipment linkage operations. Combined with real-time monitoring parameter information such as the cultivation environment and operation equipment, the operation sequence of each piece of equipment is established, and the automatic production of logistics, equipment linkage, and comprehensive configuration software are

realized. In this way, the equipment production operation control identification system and "environment-quality-yield" intelligent fine identification system are established.

In the process of optimizing the process timing using ACA [25], the Canny operator [26] is integrated into it, and a Canny-based optimized ACA is constructed. The steps of the algorithm are as follows. First, it acquires the edge heuristic information η. The improved ACA linearly combines the high and low thresholds to obtain the final threshold Th, as shown in Equation (16).

$$Th = a \times thH + b \times thL \tag{16}$$

In Equation (16), a and b are constants, thL refers to the low threshold, and thH refers to the high threshold. Usually, thH defaults to 0, and thL defaults to 0.7. Then, the heuristic information $\eta(i, j)$ of the pixel point (i, j) has a value range, as shown in Equation (17).

$$\eta(i,j) = \begin{cases} -1 & The\ point\ is\ not\ an\ edge\ point \\ [0,1] & The\ point\ is\ an\ edge\ point \end{cases} \tag{17}$$

Second, the edge tracking model of the Canny-based optimized ACA is established, and the transition probability is defined as follows according to the traditional ant colony edge detection algorithm.

$$P_i = \frac{\tau_i^{\alpha}(t)\eta_i^{\beta}(t)}{\sum\limits_{i \in S} \tau_i^{\alpha}(t)\eta_i^{\beta}(t)} \tag{18}$$

In Equation (18), α, β refers to the control factors of pheromone and heuristic information in the process of moving and is set to $\alpha = 0.6, \beta = 0.2$. $\tau_i(t)$ refers to the size of the pheromone on pixel i at the current time t. S represents the neighborhood range of the current pixel, and the transition probability is calculated in the neighborhood of S. To reduce the amount of calculation, the following equation is used:

$$\arg\max P_i = \arg\max \tau_i^{\alpha}(t)\eta_i^{\beta}(t) \tag{19}$$

In the setting of loop termination conditions, *Width* and *Height* are, respectively, the width and height of the image, and then the rate of steps that each ant is limited to walk is illustrated in Equation (20).

$$rate = Width \times Height \times dis\_rate \tag{20}$$

In Equation (20), *dis_rate* is a constant in the (0,1] interval. The path pheromone is further updated to obtain an updated objective function, as shown in Equation (21):

$$\tau_i(t+1) = (1-\rho) \times \tau_i(t) + \Delta\tau \tag{21}$$

In Equation (21), $\rho \in [0, 1]$ is the pheromone volatilization rate, and $\Delta\tau$ refers to the total amount of pheromone released by all ants at this pixel point in this cycle. The displacement matrix Q is used to cycle shift the unique seedling sample image in the target region, and the training set $\{Q_i x | i = 0, 1, \ldots, n-1\}$ is obtained. The replacement matrix Q is shown in Equation (22):

$$Q = \begin{bmatrix} 0 & 0 & \cdots & 1 \\ 1 & 0 & \cdots & 0 \\ \vdots & \vdots & \ddots & \vdots \\ 1 & 0 & \cdots & 0 \end{bmatrix} \tag{22}$$

Canny-based optimized ACA is employed to calculate the optimal timing of the process. The specific optimization process is as follows. The target loss function L is the weighted sum of the confidence error L_{conf} and the position error L_{loc}.

$$L(x, c, l, g) = \frac{1}{N}\left(L_{conf}(x, c) + \alpha L_{loc}(x, l, g)\right) \tag{23}$$

In Equation (23), c is the detection class confidence of target seedlings, l the prediction frame parameter, g the real frame parameter, and N the number of matched real frames, and α can adjust the ratio between the two types of losses, whose default value is 1. SoftMax loss is used to calculate the confidence error L_{conf}.

$$L_{conf}(x, c) = -\sum_{i \in Pos}^{N} x_{ij}^{p} \log\left(\hat{c}_j^p\right) - \sum_{i \in Neg}^{N} \log\left(\hat{c}_i^0\right) \tag{24}$$

In Equation (24), if the i-th predicted frame has a matching relationship with the j-th real frame and the matching category is p, x_{ij}^{p} equals 1; otherwise, it is 0, and confidence $\hat{c}_j^p$ is presented in Equation (25):

$$L_{loc}(x, l, g) = \sum_{i \in Pos}^{N} \sum_{m} x_{ij}^{k} smooth_{L1}\left(l_i^m - \hat{g}_j^m\right) \tag{25}$$

The calculation of $smooth_{L1}(x)$ in Equation (25) is presented in Equation (26).

$$smooth_{L1}(x) = \begin{cases} 0.5x^2 & if|x| < 1 \\ |x| - 0.5 & otherwise \end{cases} \tag{26}$$

The process of training the classifier of this model is further analyzed, as described in Equation (27):

$$\min \sum_{i=1}^{m} L(y_i, f(x_i)) + \lambda \|\omega\|^2 \tag{27}$$

That is, it finds the optimal ω so as to lowest the cost function.

$$\omega = \sum_{i} a_i \varphi(X_i) \tag{28}$$

In Equation (28), a_i corresponds to the training sample coefficient, $\varphi(X_i)$ is the function, which is utilized to map the training sample x to a high-dimensional feature space, and Equation (29) shows the relationship between x and x^* in the high-dimensional feature space.

$$\varphi^T(x)\varphi(x^*) = K(x, x^*) \tag{29}$$

In Equation (29), K refers to the Gauss adjustable function. Therefore, Equation (30) can be obtained:

$$a = (K + \lambda I)^{-1} y \tag{30}$$

In Equation (30), K is the kernel matrix constructed by the training samples $P^i x, i = 0, 1, \cdots, n-1$, $a = [a_1, a_2, \cdots, a_n]$. Fourier transform is performed on Equation (31), as follows.

$$f(a) = \hat{a} = \frac{f(y)}{f(k^{xx}) + \lambda} \tag{31}$$

In Equation (31), $\hat{a}$ is the discrete Fourier transform of a, and k^{xx} is the first-row vector of the kernel matrix K. Thus, the classifier training changes from finding the best ω to finding the optimal a.

2.4. Experiment and Evaluation Analysis

To evaluate the performance of the ANN-ACA-based plant factory seedling phenotype fine identification system, the system is generated by MATLAB simulation. Then, the vegetable lettuce in the plant factory is taken as the object, and each seedling is placed separately in rows and columns in the seedling cultivation area of the plant. Three-dimensional images of plants are obtained by using the system constructed in this work. The detailed construction details of 3D images are described in Section 2.2 above, and 408 images of 51 lettuce plants are finally obtained. The acquired image data are randomly distributed by 8:2, of which 80% are utilized for training and 20% for testing. These training samples are trained 500 times with 4 images each time, that is, 2000 iterations are carried out, that is, the model begins to converge, the loss of the verification sample begins to rise, and the loss of the training sample is fixed in a certain area. The PyTorch training framework, Intel Core i7 processor, 11 GB video memory, 1080 Ti GPU, and 16 GB memory computer are used for training.

The proposed model algorithm is compared with R-CNN [27], SPPNet [28], Fast R-CNN [29], Faster R-CNN [30], and MRCNN proposed by others. The phenotypes of plants are analyzed for accuracy according to four stages, including the germination stage, seedling stage, rosette stage, and heading stage, and the time required for the training and test data set is analyzed.

For the optimization evaluation of the process timing, the optimized ACA proposed is analyzed in contrast to the genetic algorithm (GA) [31], ACA [32], particle swarm optimization (PSO) [33], and methodology of Hou et al. (2022) [34].

3. Results and Discussion

3.1. System Performance Analysis

To reduce model losses, various optimizers and learning rates (LRs) are screened to optimize system performance. The selected optimizers are the standard gradient descent (GD), stochastic GD (SGD), batch GD (BGD), RMSprop algorithm, and Adam algorithm. For the LR, cosine annealing attenuations LR, exponential attenuations LR, fixed-step attenuations LR, multistep attenuations LR, and fixed value LR = 0.0001 are selected for comparison. The training and test results are illustrated in Figure 6.

Figure 6a,b illustrate the optimization effects of various optimizers. Figure 6a is the loss trend of the training set, and Figure 6b is that of the test set. The training loss reaches the minimum when the RMSprop optimizer is used, followed by Adam, while the loss values of GD, BGD, and SGD are basically the same, but SGD reaches the convergence loss value the fastest. Although the RMSprop optimizer achieves an optimal training loss, the test loss is minimized when using the Adam optimizer. Therefore, the Adam optimizer has the best effect when constructing the model in this work.

Figure 6c,d show the results of training loss and validation loss using iterative methods with different learning rates, respectively. Both training loss and test loss fluctuate and decrease. However, when the exponential decay learning rate iteration method is used, both training loss and test loss reach the lowest value faster than when other learning rate iteration methods are used, and the loss is minimal. Therefore, the exponential decay learning rate iteration method is chosen.

3.2. Comparison of Phenotype Recognition Accuracy of Seedlings in Plant Factories under Different Algorithms

Each algorithm is used to accurately identify and analyze the phenotypes of the seedlings according to the four stages: germination stage, seedling stage, rosette stage, and heading stage (Figure 7).

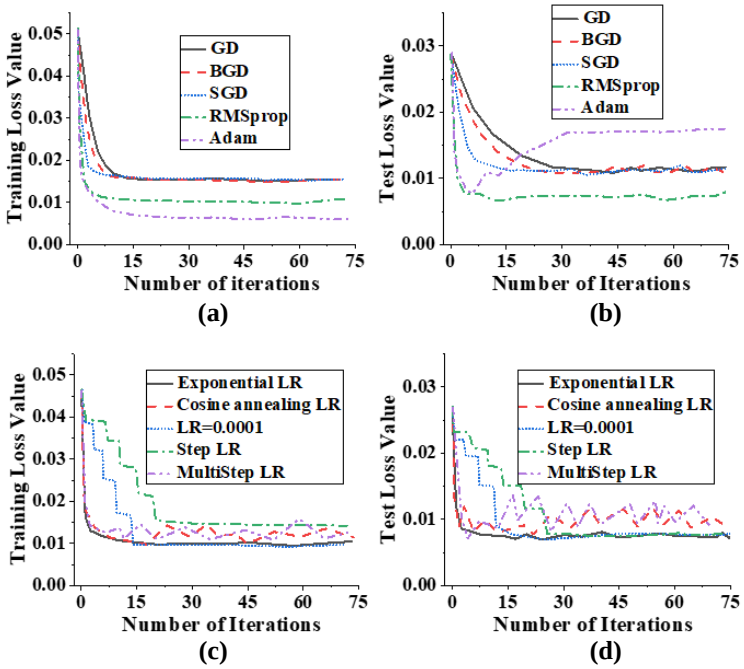

Figure 6. Contrast graph of training and test results under different overparameters. (**a**) Training losses with different optimizers; (**b**) test losses from using different optimizers; (**c**) training losses caused by iterative methods with different learning rates; (**d**) test loss with iterative methods of different learning rates.

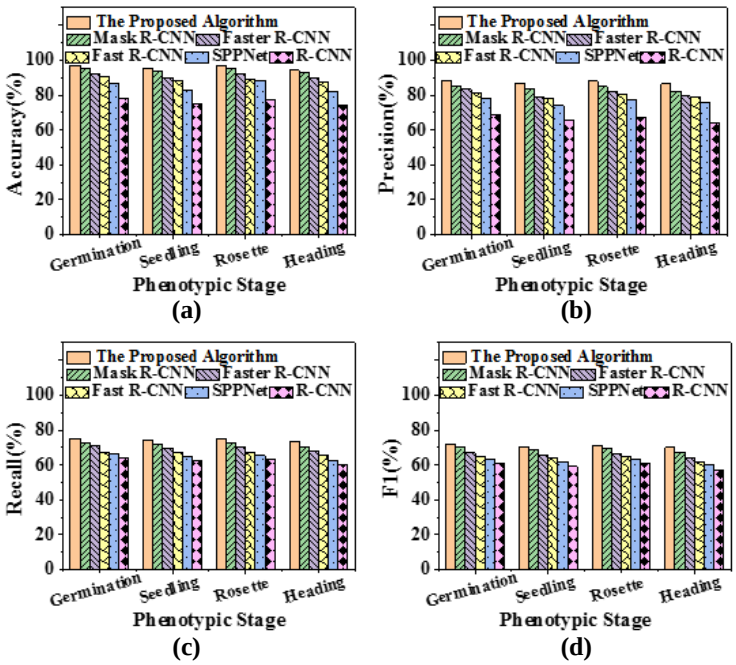

Figure 7. Recognition accuracy map of each phenotypic stage of plants under different algorithms (**a**) accuracy; (**b**) precision; (**c**) recall; (**d**) F1.

Accuracy, precision, recall, and F1 of this system model and other algorithms in analyzing the phenotypes of the four stages of plant germination stage, seedling stage, rosette stage, and heading stage are compared (Figure 7). Among the four stages, the phenotypic recognition accuracy of the germination stage is significantly better than that of the other stages, and it may be that the identification of plants from scratch is the most significant. From the comparison of different algorithms, the proposed model algorithm

has a recognition accuracy of 97.01% in the germination stage, which is 1.55% superior to the model algorithms proposed by others. Furthermore, comparisons show that the precision, recall, and F1 of this model algorithm in the germination stage are 88.42%, 75.57%, and 72.13%, respectively, which are significantly higher than those of the other algorithms. Hence, the phenotype recognition and prediction accuracy of the ANN-ACA-based plant factory seedling phenotype fine identification system is superior.

The comparison of time required for phenotype recognition of each algorithm is illustrated in Figure 8.

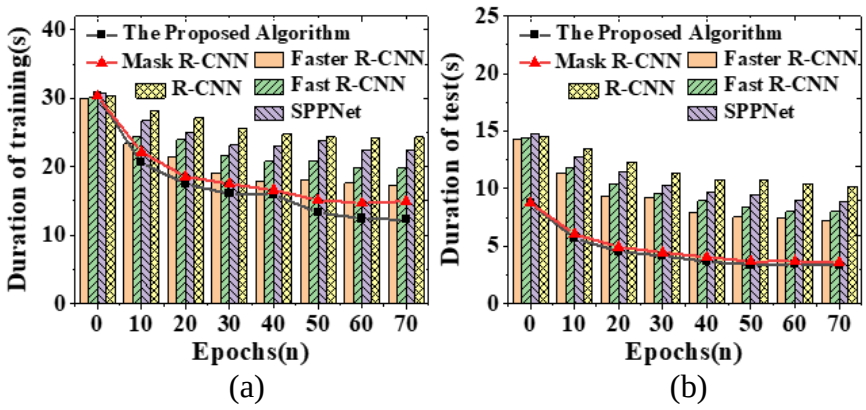

Figure 8. Comparison curves of the time required for phenotype recognition of various algorithms (**a**) training time; (**b**) testing time.

With the increase in iterations, a trend of decreasing first and then basically remaining unchanged is demonstrated both in the required training duration and test duration, that is, reaching convergence. The training duration and test duration of the proposed model are stable at 12.26 s and 5.64 s, respectively. Moreover, the model algorithm constructed in this work requires markedly less time for prediction than other models. Therefore, the establishment of the ANN-ACA-based plant factory seedling phenotype fine identification system can achieve a high phenotype recognition and prediction effect in a shorter time.

3.3. Process Optimization and Data Transmission Performance Analysis of Plant Factories under Different Algorithms

The comparison results of plant factory process optimization and data transmission performance under different algorithms are shown in Figures 9 and 10, respectively.

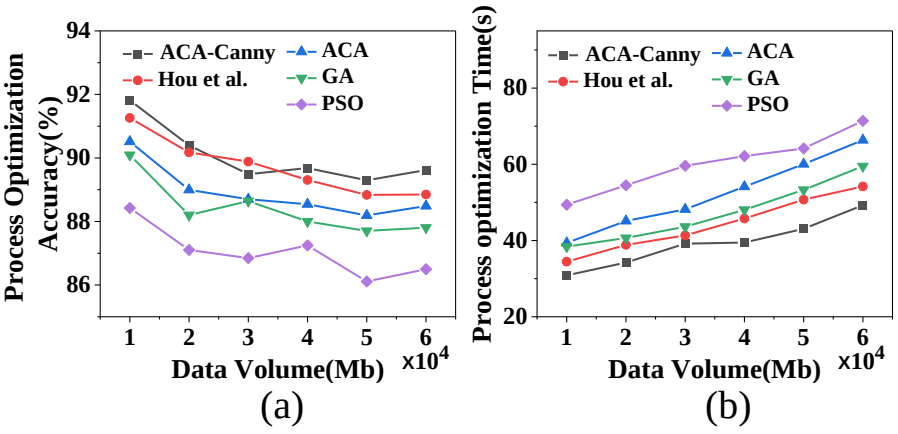

Figure 9. Curves of process optimization accuracy and required time of plant factory under different data amounts (**a**) process optimization accuracy; (**b**) required time.

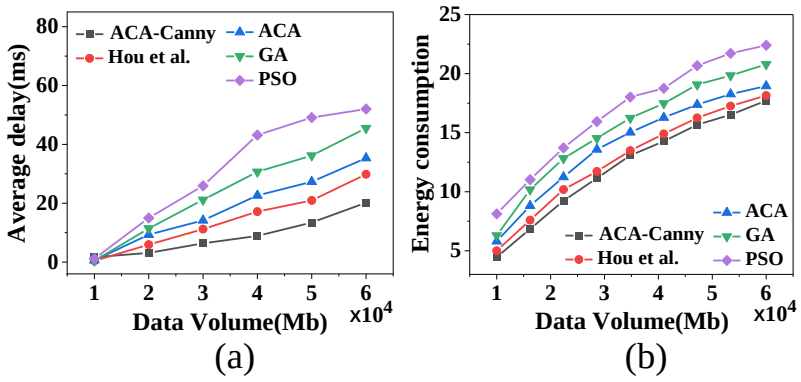

Figure 10. Energy consumption and delay changes in algorithms under various data amounts (**a**) delay; (**b**) energy consumption.

Figure 9a illustrates that the process optimization accuracy of each algorithm is analyzed under different data amounts. The proposed Canny-based ACA can keep the process timing optimization accuracy at approximately 90.26% in the plant factory, while the accuracy of other algorithms is lower than 89.89%. At the same time, the optimization accuracy of each algorithm from high to low is the proposed model algorithm > Hou et al. (2022) > ACA > GA > PSO. From Figure 9b, the model algorithm proposed is considerably lower than other models regarding the time required for process optimization. When the amount of data is 6000 Mb, the required time is 49.26 s. Moreover, the required time of each algorithm is in the order of the proposed model algorithm < Hou et al. (2022) < ACA < GA < PSO from short to long. Therefore, the proposed algorithm model can optimize the process timing in the plant factory to high accuracy in a relatively short time.

The time delay and energy consumption analysis of the data transmission of the three algorithms are expounded in Figure 10. With an increased data amount, the required energy consumption and delay both show an upward trend. The delay and energy consumption of the proposed model algorithm is stable at 20.17 ms and 17.71 ms, respectively, when the data are 6000 Mb, which is notably inferior to the delay and energy consumption of other models. The average time delay and energy consumption of each algorithm are in the order of the proposed model algorithm < Hou et al. (2022) < ACA < GA < PSO from small to large. Therefore, the constructed ANN-ACA-based plant factory seedling phenotype fine identification system can optimize the process timing in a more real-time manner with lower energy consumption.

3.4. Discussion

In this work, a plant factory seedling phenotype fine management system based on ANN-ACA is constructed. In the performance analysis of the system, ablation experiments are conducted from the perspective of optimizer selection and learning rate iteration. The system demonstrates the best performance when the Adam optimizer and exponential decay learning rate iteration are used. This is consistent with the views of Xu et al. (2021) [35]. In the analysis of seedling phenotype recognition accuracy at different stages, it is found that the phenotype recognition precision in the germination stage is significantly better than that in other stages, which might be the most significant in plant-from-scratch recognition. Moreover, the precision, recall, and F1 of the germination stage are 88.42%, 75.57%, and 72.13%, respectively, drastically superior to those of the other algorithms. However, the identification accuracy of the seedling stage, rosette stage, and pelleting stage was lower than that of the germination stage, which is consistent with the results obtained by Hati and Singh (2021) [36]. Further comparative analysis of plant process optimization and data transmission performance under different algorithms shows that the process timing optimization accuracy of the proposed model algorithm is maintained at 90.26%, and the time delay and energy consumption are stabilized at 20.17 ms and 17.71, respectively, when the data volume is 6000 Mb. This further verifies the accuracy of the proposed algorithm in

data transmission rate and process timing optimization, which is similar to the study of Zhou et al. (2022) [37]. Thus, the model constructed in this work can effectively identify the phenotype of seedlings in plant factories and carry out fine management of their processes.

4. Conclusions

Today, the application field of artificial intelligence technology is increasingly extensive. Aiming at the problems of confused identification of plant phenotype, many production links, and complicated process equipment in the existing plant factory, the MRCNN algorithm is introduced to analyze plant phenotype, and the process sequence in the plant factory is optimized through the optimized ACA, thus constructing a fine management system of plant factory seedling phenotype based on ANN-ACA. Experimental analysis suggests that this research algorithm can accurately identify the plant phenotype, and the recognition accuracy reaches 97.01% and can optimize the relationship of the plant process sequence according to the phenotype, which can provide an example for the progression of intelligent management systems and complete equipment integration in unmanned plant factories in the later stage. However, there are some shortcomings in this work, such as identifying plant phenotypic information efficiently by constructing 3D images, in which it is assumed that a point on a plant is visible in all camera views. However, in practical problems, there may be some plants that cannot be photographed by occlusion cameras because many plants share the same shooting system, so the solution to the occlusion problem can be studied later. At the same time, in later work, a separation machine can be designed for different kinds of plants, which makes the culture system of different seedlings more focused. In addition, the MRCNN algorithm and optimized ACA are introduced to build the model system, but the influence and combination of the two algorithms are not considered. Therefore, the combination of the MRCNN algorithm and ant colony optimization algorithm can be further promoted in follow-up work, and the performance of the seedling phenotype fine management system in plant factories can be further improved.

Author Contributions: Conceptualization, K.C. and Y.Z.; methodology, K.C.; software, B.Z.; validation, B.Z., L.Z. and Y.Z.; formal analysis, K.C.; investigation, K.C.; resources, Y.Z.; data curation, Y.Z.; writing—original draft preparation, K.C.; writing—review and editing, K.C. All authors have read and agreed to the published version of the manuscript.

Funding: This research was funded by the National Key Research and Development Program of China Sub-project grant number [No. 2021YFD2000705]. And The APC was funded by [No. 2021YFD2000705].

Institutional Review Board Statement: Not applicable.

Data Availability Statement: No data were used for the research described in the article.

Conflicts of Interest: The authors declare no conflict of interest.

References

1. Menshchikov, A.; Shadrin, D.; Prutyanov, V.; Lopatkin, D.; Sosnin, S.; Tsykunov, E.; Somov, A. Real-time detection of hogweed: Uav platform empowered by deep learning. *IEEE Trans. Comput.* **2021**, *70*, 1175–1188. [CrossRef]
2. Nagano, S.; Moriyuki, S.; Wakamori, K.; Mineno, H.; Fukuda, H. Leaf-movement-based growth prediction model using optical flow analysis and machine learning in plant factory. *Front. Plant Sci.* **2019**, *10*, 227. [CrossRef] [PubMed]
3. Wang, X.; Xuan, H.; Evers, B.; Shrestha, S.; Pless, R.; Poland, J. High-throughput phenotyping with deep learning gives insight into the genetic architecture of flowering time in wheat. *GigaScience* **2019**, *8*, giz120. [PubMed]
4. Yang, W.; Yang, C.; Hao, Z.; Xie, C.; Li, M. Diagnosis of plant cold damage based on hyperspectral imaging and convolutional neural network. *IEEE Access* **2019**, *7*, 118239–118248. [CrossRef]
5. Arya, S.; Sandhu, K.S.; Singh, J. Deep learning: As the new frontier in high-throughput plant phenotyping. *Euphytica* **2022**, *218*, 47. [CrossRef]
6. Moghimi, A.; Yang, C.; Marchetto, P.M. Ensemble feature selection for plant phenotyping: A journey from hyperspectral to multispectral imaging. *IEEE Access* **2018**, *6*, 56870–56884. [CrossRef]

7. Zhang, R.; Song, S.; Wu, C. Robust scheduling of hot rolling production by local search enhanced ant colony optimization algorithm. *IEEE Trans. Ind. Inform.* **2019**, *16*, 2809–2819. [CrossRef]
8. Waqar, A.; Subramaniam, U.; Farzana, K.; Elavarasan, R.M.; Habib HU, R.; Zahid, M.; Hossain, E. Analysis of optimal deployment of several DGs in distribution networks using plant propagation algorithm. *IEEE Access* **2020**, *8*, 175546–175562. [CrossRef]
9. Zhang, H.; Zhang, C.; Peng, Y.; Wang, D.; Tian, G.; Liu, X.; Peng, Y. Balancing problem of stochastic large-scale U-type assembly lines using a modified evolutionary algorithm. *IEEE Access* **2018**, *6*, 78414–78424. [CrossRef]
10. Jin, S.; Su, Y.; Gao, S.; Wu, F.; Ma, Q.; Xu, K.; Guo, Q. Separating the structural components of maize for field phenotyping using terrestrial LiDAR data and deep convolutional neural networks. *IEEE Trans. Geosci. Remote Sens.* **2019**, *58*, 2644–2658. [CrossRef]
11. Wu, C.; Zeng, R.; Pan, J.; Wang, C.C.; Liu, Y.J. Plant phenotyping by deep-learning-based planner for multi-robots. *IEEE Robot. Autom. Lett.* **2019**, *4*, 3113–3120. [CrossRef]
12. Nesteruk, S.; Shadrin, D.; Pukalchik, M.; Somov, A.; Zeidler, C.; Zabel, P.; Schubert, D. Image compression and plants classification using machine learning in controlled-environment agriculture: Antarctic station use case. *IEEE Sens. J.* **2021**, *21*, 17564–17572. [CrossRef]
13. Yang, X.; Xi, Z.; Li, J.; Feng, X.; Zhu, X.; Guo, S.; Song, C. Deep Transfer Learning-Based Multi-Object Detection for Plant Stomata Phenotypic Traits Intelligent Recognition. *IEEE/ACM Trans. Comput. Biol. Bioinform.* **2021**, *20*, 321–329. [CrossRef] [PubMed]
14. Lv, Z.; Qiao, L. Deep belief network and linear perceptron based cognitive computing for collaborative robots. *Appl. Soft Comput.* **2020**, *92*, 106300. [CrossRef]
15. Fujimoto, Y.; Murakami, S.; Kaneko, N.; Fuchikami, H.; Hattori, T.; Hayashi, Y. Machine learning approach for graphical model-based analysis of energy-aware growth control in plant factories. *IEEE Access* **2019**, *7*, 32183–32196. [CrossRef]
16. Zheng, J.; Ji, F.; He, D.; Niu, G. Effect of light intensity on rooting and growth of hydroponic strawberry runner plants in a LED plant factory. *Agronomy* **2019**, *9*, 875. [CrossRef]
17. An, S.; Hwang, H.; Chun, C.; Jang, Y.; Lee, H.J.; Wi, S.H.; Kwack, Y. Evaluation of air temperature, photoperiod and light intensity conditions to produce cucumber scions and rootstocks in a plant factory with artificial lighting. *Horticulturae* **2021**, *7*, 102. [CrossRef]
18. Hyunjin, C.; Sainan, H. A study on the design and operation method of plant factory using artificial intelligence. *Nanotechnol. Environ. Eng.* **2021**, *6*, 41. [CrossRef]
19. Demidchik, V.V.; Shashko, A.Y.; Bandarenka, U.Y.; Smolikova, G.N.; Przhevalskaya, D.A.; Charnysh, M.A.; Medvedev, S. Plant phenomics: Fundamental bases, software and hardware platforms, and machine learning. *Russ. J. Plant Physiol.* **2020**, *67*, 397–412. [CrossRef]
20. Paulus, S.; Mahlein, A.K. Technical workflows for hyperspectral plant image assessment and processing on the greenhouse and laboratory scale. *GigaScience* **2020**, *9*, giaa090. [CrossRef]
21. Lyu, S.; Noguchi, N.; Ospina, R.; Kishima, Y. Development of phenotyping system using low altitude UAV imagery and deep learning. *Int. J. Agric. Biol. Eng.* **2021**, *14*, 207–215. [CrossRef]
22. Liu, Y.; Ma, X.; Shu, L.; Hancke, G.P.; Abu-Mahfouz, A.M. From Industry 4.0 to Agriculture 4.0: Current status, enabling technologies, and research challenges. *IEEE Trans. Ind. Inform.* **2020**, *17*, 4322–4334. [CrossRef]
23. Zou, W.Q.; Pan, Q.K.; Tasgetiren, M.F. An effective discrete artificial bee colony algorithm for scheduling an automatic-guided-vehicle in a linear manufacturing workshop. *IEEE Access* **2020**, *8*, 35063–35076. [CrossRef]
24. Wan, J.; Chen, B.; Wang, S.; Xia, M.; Li, D.; Liu, C. Fog computing for energy-aware load balancing and scheduling in smart factory. *IEEE Trans. Ind. Inform.* **2018**, *14*, 4548–4556. [CrossRef]
25. Li, H.; Wang, Y.; Fan, F.; Yu, H.; Chu, J. Sustainable Plant Layout Design for End of Life Vehicle Recycling and Disassembly Industry Based on SLP Method, a Typical Case in China. *IEEE Access* **2021**, *9*, 81913–81925. [CrossRef]
26. Lu, C.; Gao, L.; Yi, J.; Li, X. Energy-efficient scheduling of distributed flow shop with heterogeneous factories: A real-world case from automobile industry in China. *IEEE Trans. Ind. Inform.* **2020**, *17*, 6687–6696. [CrossRef]
27. Han, C.; Li, G.; Ding, Y.; Yan, F.; Bai, L. Chimney detection based on faster R-CNN and spatial analysis methods in high resolution remote sensing images. *Sensors* **2020**, *20*, 4353. [CrossRef]
28. Yin, G.; Xie, Y.; Yun, J.; Ning, L.; Liu, Y. Fruit target detection method based on faster R-CNN. *Int. J. Wirel. Mob. Comput.* **2021**, *21*, 207–213. [CrossRef]
29. Lu, W.; Du, R.; Niu, P.; Xing, G.; Luo, H.; Deng, Y.; Shu, L. Soybean Yield Preharvest Prediction Based on Bean Pods and Leaves Image Recognition Using Deep Learning Neural Network Combined With GRNN. *Front. Plant Sci.* **2022**, *12*, 791256. [CrossRef] [PubMed]
30. Wei, T.J.; Chang, S.W.; Abdul-Kareem, S.; Yap, H.J.; Yong, K.T. Deep learning for plant species classification using leaf vein morphometric. *IEEE/ACM Trans. Comput. Biol. Bioinform.* **2018**, *17*, 82–90.
31. Zhou, H.; Yang, C.; Sun, Y. A Collaborative Optimization Strategy for Energy Reduction in Ironmaking Digital Twin. *IEEE Access* **2020**, *8*, 177570–177579. [CrossRef]
32. Liu, C.; Wu, L.; Huang, X.; Xiao, W. Improved dynamic adaptive ant colony optimization algorithm to solve pipe routing design. *Knowl. Based Syst.* **2022**, *237*, 107846. [CrossRef]
33. Su, B.; Lin, Y.; Wang, J.; Quan, X.; Chang, Z.; Rui, C. Sewage treatment system for improving energy efficiency based on particle swarm optimization algorithm. *Energy Rep.* **2022**, *8*, 8701–8708. [CrossRef]

34. Hou, J.; Zhang, J.; Wu, W.; Jin, T.; Zhou, K. Research on agricultural machinery rental optimization based on the dynamic artificial bee-ant colony algorithm. *Algorithms* **2022**, *15*, 88. [CrossRef]
35. Xu, C.; Liu, S.; Yang, Z.; Huang, Y.; Wong, K.K. Learning rate optimization for federated learning exploiting over-the-air computation. *IEEE J. Sel. Areas Commun.* **2021**, *39*, 3742–3756. [CrossRef]
36. Hati, A.J.; Singh, R.R. Artificial intelligence in smart farms: Plant phenotyping for species recognition and health condition identification using deep learning. *AI* **2021**, *2*, 274–289. [CrossRef]
37. Zhou, X.; Ma, H.; Gu, J.; Chen, H.; Deng, W. Parameter adaptation-based ant colony optimization with dynamic hybrid mechanism. *Eng. Appl. Artif. Intell.* **2022**, *114*, 105139. [CrossRef]